since 1961

Baltica

BALTICA Volume 39 Number 1 June 2026: 1–15
https://doi.org/10.5200/baltica.2026.1.1

Research article

Seismic attributes for enhancing fault detection and assessing the risk of water invasion: a case study from Concession 82, Sirte Basin, Libya

Nureddin Saadi, Osama Shtawei

Saadi, N., Shtawei, O. 2026. Seismic attributes for enhancing fault detection and assessing the risk of water invasion: a case study from Concession 82, Sirte Basin, Libya. *Baltica 39 (1)* 1–15. Vilnius. ISSN 0067-3064.
Manuscript submitted 13 June 2025 /Accepted 17 December 2025 / Available online 10 February 2026

Abstract. This study aimed to investigate the structural configuration of the reservoir in Concession 82, located in the Sirte Basin, Libya, with a particular emphasis on identifying faults and associated fractures that contributed to water invasion during drilling operations in one of the wells within the study area. The methodology involved the application of the ant tracking seismic attribute to extract lineaments indicative of fault structures. Several faults and fractures were successfully identified and delineated in the vicinity of the non-productive well. A statistical analysis of the extracted faults was conducted to assess variations in fault trends and density across the study area. The findings revealed that the non-productive well was drilled directly along a fault plane, which facilitated water invasion. The inability to detect this fault prior to drilling was attributed to the poor quality of the original seismic data. Further analysis demonstrated that the study area is characterized by a complex fault system exhibiting a range of orientations, magnitudes, and depths. This finding is consistent with and supports several previous studies on the tectonic and structural evolution of the Sirte Basin. Understanding these fault characteristics is crucial for mitigating drilling risks such as water invasion. Notably, the failure of the non-productive well is directly linked to the presence of the identified fault. Despite this issue, the structural configuration of the area suggests a strong potential for hydrocarbon accumulation.

Keywords: *ant tracking algorithm; variance attribute analysis; water breakthrough; structural interpretation; hydrocarbon reservoir*

Nureddin Saadi (n.saadi@uot.edu.ly), https://orcid.org/0000-0003-0593-8578;
Department of Geological Engineering, Faculty of Engineering, University of Tripoli, Libya;
Osama Shtawei (o.o.s.shtawei@gmail.com), https://orcid.org/0009-0004-0624-8784;
Department of Geological & Geophysical, Mellitah Oil & Gas B.V., Libya

INTRODUCTION

Despite substantial advancements in exploration technology, the risk of drilling a dry oil or gas well remains a persistent challenge. One of the primary causes of such outcomes is the presence of faults and fractures within the subsurface formations, which can result in the migration or loss of hydrocarbons (Azzam *et al*. 2018; Shoup 2019). When a drill bit intersects a fault or fracture, hydrocarbons may escape, rendering the well non-productive. In some instances, these structural discontinuities may be too subtle to detect using conventional seismic data, complicating efforts to avoid them.

Fault interpretation plays a critical role in constructing accurate seismic models that guide field development(Zou *et al*. 2023). It is important to note that faults and fractures are not always desirable during drilling operations, as they can significantly influence fluid flow dynamics, potentially leading to early water breakthrough in hydrocarbon reservoirs (Abdullah *et al*. 2020; Fernandez-Ibanez *et al.* 2022).

This paper presents the application of a fault-detection technology designed to reduce uncertainties and minimize risk in high-cost drilling operations (Popovici *et al*. 2017). A well located in Concession 82, Sirte Basin, experienced water invasion during the drilling phase. The primary hydrocarbon production in this concession is derived from the Upper Cretaceous Rakb Formation, which represents the main

reservoir within the study area (Shaltami *et al*. 2025). In this case, the available seismic dataset was of poor quality, posing significant challenges for fault identification and interpretation.

The objective of this study is to extract, interpret, and evaluate fault systems by using seismic and GIS-based techniques enabling correlation of fault features between two wells – one productive and one non-productive. The goal is to enhance well placement strategies and mitigate structural risks such as water invasion during drilling.

Fault detection was conducted using seismic variance attributes (Jaglan *et al*. 2015). The interpreted fault structures were validated by cross-referencing the attribute-derived results with the original seismic data. Ant Tracking, a technique implemented in Petrel software, was also employed to enhance fault delineation (Kim *et al*. 2021). The preprocessing workflow included structural smoothing and filtering of seismic data, followed by attribute extraction. The Ant Tracking algorithm utilizes autonomous agents ("ants") that trace faults by navigating seismic discontinuities while minimizing interference from noise.

Seismic interpretation plays a critical role in identifying fault structures that influence hydrocarbon exploration and production. Traditional seismic interpretation methods often face challenges due to the varying quality of seismic data, which can limit the detection of subtle or complex fault features. In recent years, attribute-based fault detection techniques have been developed to enhance fault identification by extracting detailed structural information from seismic datasets. The Sirte Basin, a region of significant tectonic complexity and hydrocarbon potential, presents an ideal case study for applying these advanced methods. Understanding fault trends and orientations within the basin is essential for optimizing well placement and mitigating risks such as water invasion, which can adversely affect reservoir performance. This study aims to evaluate the effectiveness of attribute-based fault detection compared to conventional interpretation approaches and to provide insights into the structural framework of the Sirte Basin to support future exploration and development efforts. Due to confidentiality agreements, sensitive information such as geographic coordinates and well identifiers are withheld to protect proprietary data from involved oil and gas companies.

Due to confidentiality obligations, specific details such as geographic coordinates and well names cannot be disclosed. All data collected and analyzed during this research were handled in accordance with confidentiality agreements to safeguard proprietary information belonging to oil and gas companies in Libya.

GEOLOGICAL SETTING

The study area is situated in the eastern part of the Sirte Basin, specifically within the Sarir Trough, a region characterized by significant hydrocarbon accumulations associated with structural highs and grabens formed during rifting events (Fig. 1). The Sirte Basin is widely regarded as a classic example of a continental rift system and is considered a segment of the broader Tethyan rift system (Futyan, Jawzi 1996; Guiraud, Bosworth 1997). The region's structural complexity is underscored by recurrent cycles of uplift and subsidence, beginning in the late Precambrian with the Pan-African orogeny – a major tectonic event that amalgamated early continental fragments to form the supercontinent Gondwanaland (Kroner 1993).

The underlying folded basement consists of Pan-African (Precambrian) crystalline rocks, with compressional fabrics clearly visible on deep seismic reflectors. In contrast, the overlying sedimentary succession predominantly exhibits extensional structures. Our seismic interpretation reveals intense fracturing and faulting within the deeper Rakb-C6 interval and the units beneath it, while the overlying Rakb-C5 and younger intervals show significantly lower fracture density. This suggests that the primary phase of brittle deformation mainly affected the deeper syn-rift packages.

Rifting activity in the area commenced during the Early Cretaceous, intensified throughout the Late Cretaceous, and concluded in the Early Tertiary. This tectonic evolution culminated in the formation of a triple junction involving the Sirte, Tibesti, and Sarir arms (Fig. 2) (Harding 1984; Gras, Thusu 1998; Ambrose 2000). According to Anketell (1996), the Early Cretaceous rifting phase was influenced by east-west-oriented sinistral (left-lateral) strike-slip fault zones, which significantly affected sediment deposition in the Sarir arm. However, Ambrose (2000) proposed that dextral (right-lateral) shear forces were more influential during this deformation phase. By the Late Cretaceous, dextral shear had become the dominant tectonic force, as supported by the findings of Gras (1996), Guiraud and Bosworth (1997), and Ambrose (2000). This tectonic regime led to the development of a series of northwest-trending horsts and grabens that exhibit a gradual structural descent toward the east.

The complex tectonic history of the Sirte Basin fostered the formation of numerous hydrocarbon reservoirs and created favourable conditions for hydrocarbon generation, migration, and entrapment, particularly in association with horst blocks. The basin is underpinned by a single dominant petroleum system, known as the Sirte-Zelten Total Petroleum System.

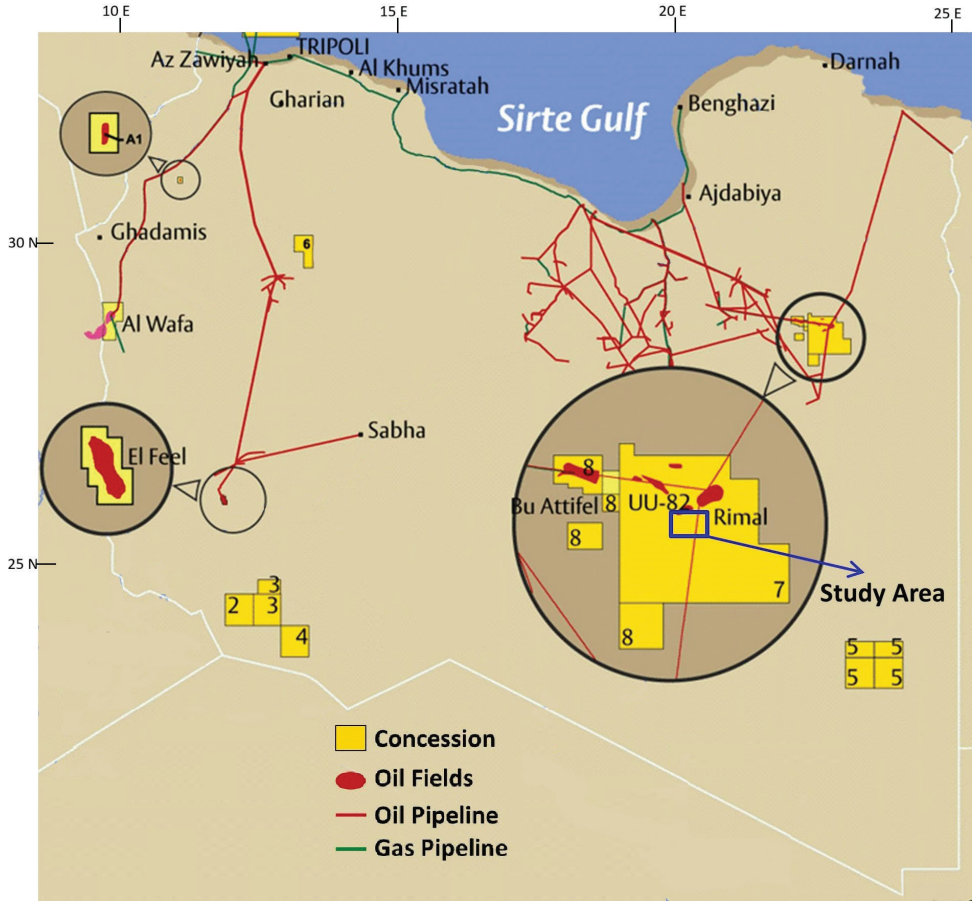

Fig. 1 Map of Libya's oil fields, showing the study area (blue rectangle) located in the Sarir Trough, eastern Sirte Basin – a major rift-related hydrocarbon province characterized by structural highs and extensional grabens (after MOGCO 2019)

This naming convention follows the framework established by Magoon and Dow (1994), which links the petroleum system name to the primary source rock – in this case, the Upper Cretaceous (Senonian/Campanian) Sirte Shale of the Rakb Group (Fig. 3). Some researchers distinguish between the Upper Sirte Shale (Campanian) and the Lower Sirte Shale (Turonian), separated by the Tagrifet Limestone (Coniacian/Santonian), with all three units recognized as effective source rocks (Mansour, Magairhy 1996). The seismic data indicates that normal faults offset the Rakb-C6 and older units but terminate beneath the Rakb-C5, which remains undeformed. This stratigraphic relationship constrains the main rift-related deformation to the Late Jurassic – Early Cretaceous syn-rift stage. Deposition of the Rakb-C5 marks the waning of rift activity, after which the basin entered a post-rift thermal subsidence phase during the Paleogene – Recent (Anketell 1996).

METHODOLOGY AND DATA ANALYSIS

The seismic data used in this study was acquired in the 1980s. The dataset underwent multiple processing stages, ultimately resulting in an updated Pre-Stack

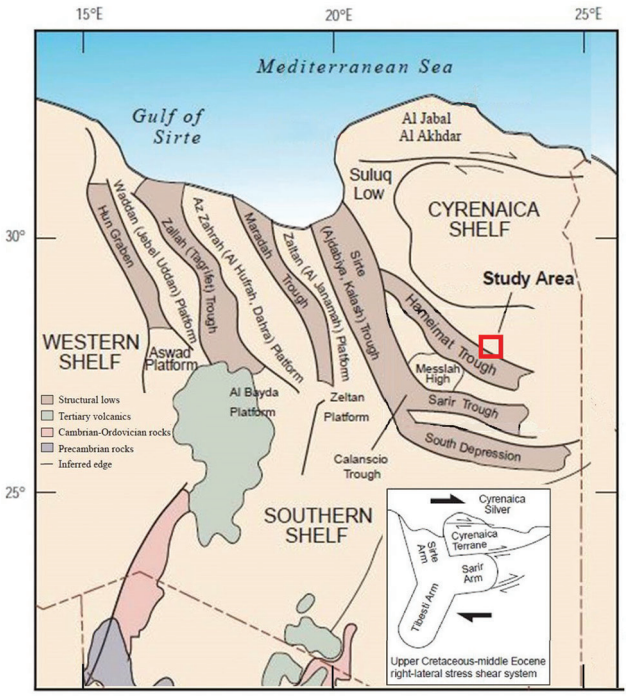

Fig. 2 Major structural elements of the Sirte Basin, highlighting its rift-related architecture of horsts and grabens formed during Cretaceous – Early Tertiary rifting. The basin represents a failed arm of a triple junction that includes the Sirte, Tibesti, and Sarir rift arms (after Ahlbrandt 2001). The study area is outlined with a red rectangle

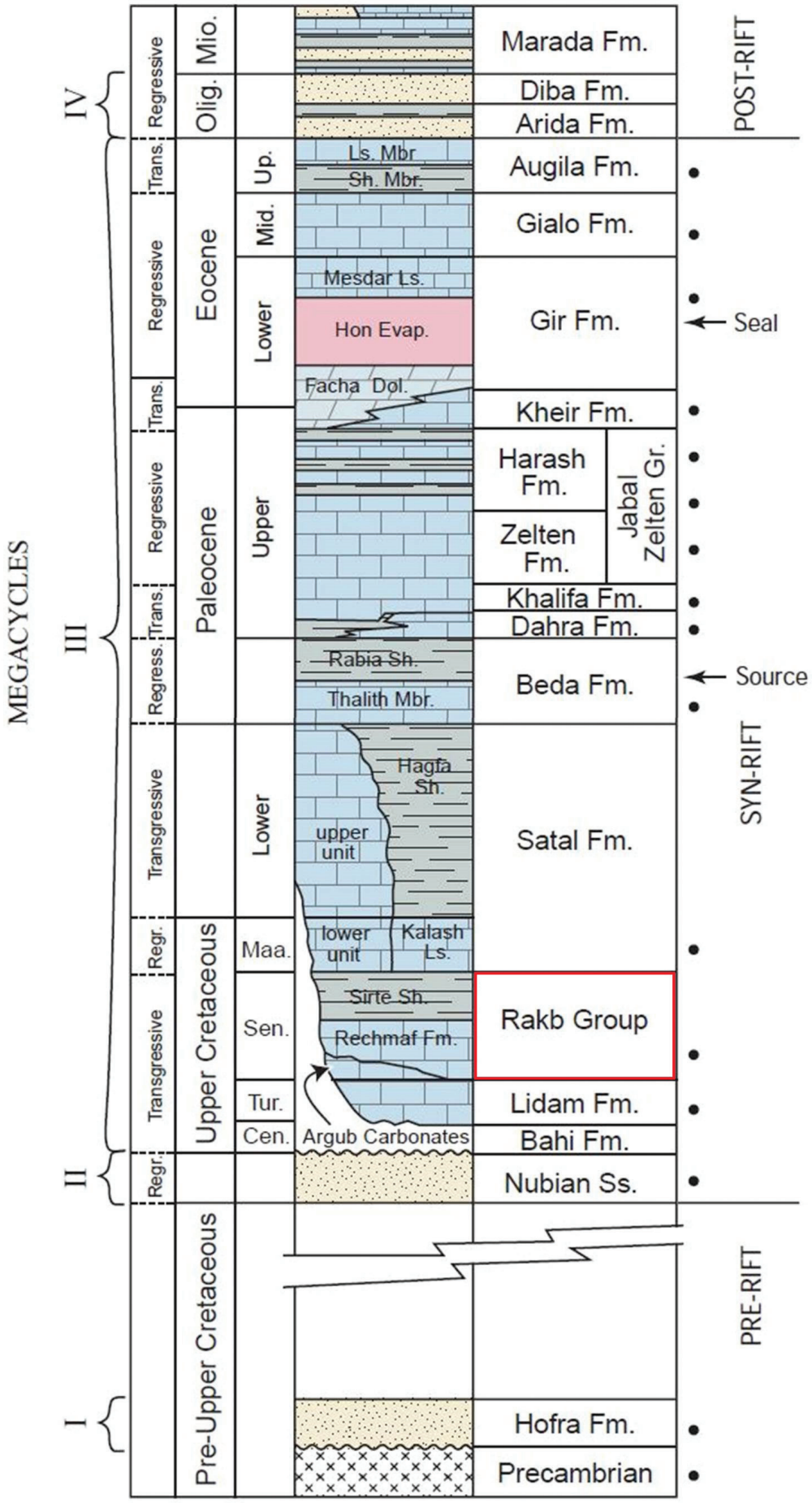

Fig. 3 Stratigraphic profile of the central Sirte Basin, highlighting the primary source rocks (Sirte Shale) and regional seal units. Reservoirs are indicated by dots (Ahlbrandt 2001). The RC-8 Rakb reservoir, which is the focus of this study, is specifically marked in the stratigraphic column

Depth Migrated (PSDM) cube. Figure 4 displays the seismic coverage of the study area, including the locations of both the productive and non-productive wells. Figure 5 presents the NW-SE seismic section illustrating the wells in relation to adjacent faults and reservoir depths. The initial seismic data were of suboptimal quality, likely due to limitations inherent in the original acquisition process. To address these deficiencies, several enhancement techniques were applied. Specifically, a median filter was employed to improve the quality and interpretability of the seismic data (Liu 2013; Onajite 2014).

The median filter was used to enhance post-stack seismic characteristics by equalizing amplitudes across the seismic cube, thereby improving data continuity and consistency. This filter played a crucial role in reducing the random noise in the seismic data that can introduce misleading linear features resembling faults. The application of the median filter effectively reduced these artificial patterns, preserving the integrity of true geological structures. This filtering process constituted a preparatory step before applying the Ant Tracking attribute.

Despite these enhancements, the seismic data still required further optimization to reach the desired level of clarity for structural interpretation. During the Ant Tracking process, a technique used for automatic fault detection, a directional constraint was applied to prevent the algorithm from detecting false faults aligned with the orientation of the seismic survey lines. This measure helped ensure that fault detection was geologically valid and minimized the risk of generating misleading features.

Before applying the enhancement techniques, two crossline seismic sections, both oriented SW–NE, were generated to identify faults affecting the investigated wells. These preliminary interpretations were subsequently compared with results from the processed dataset (Figs 6, 7, 8). Figure 8 strongly suggests that the non-productive well is located on the downthrown side of a major fault (highlighted in red), which may be responsible for the observed water invasion. However, this hypothesis necessitates further validation through advanced seismic attribute analysis.

Seismic variance attributes

The seismic variance attribute quantifies the degree of variation in seismic amplitude within a specified time window or depth interval. It is computed by calculating the statistical variance of seismic amplitudes within the designated interval. This attribute is particularly useful in highlighting areas of high and low amplitude variability, which can be indicative of geological structures such as faults, fractures, and stratigraphic discontinuities (Abdalla 2021). Specifically, high variance values often correspond to faulted or structurally complex zones, whereas low variance values are typically associated with more uniform geological formations.

The seismic variance attribute is widely employed in seismic interpretation workflows to assist in the identification and characterization of subsurface geological features. Among seismic attributes, variance is considered one of the most effective for detecting fault edges and discontinuities. It is particularly use-

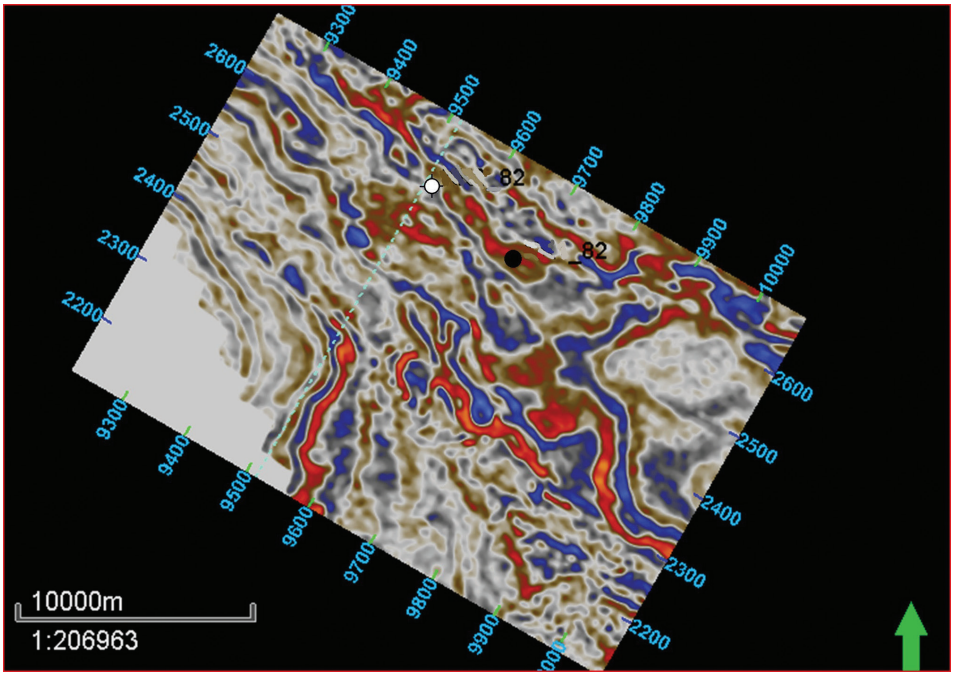

Fig. 4 Seismic slice viewed from the top of the original 3D seismic cube, at a depth equivalent to the top of the RC8 reservoir surface. It shows the locations of the productive well (black circle) and the non-productive well (white circle)

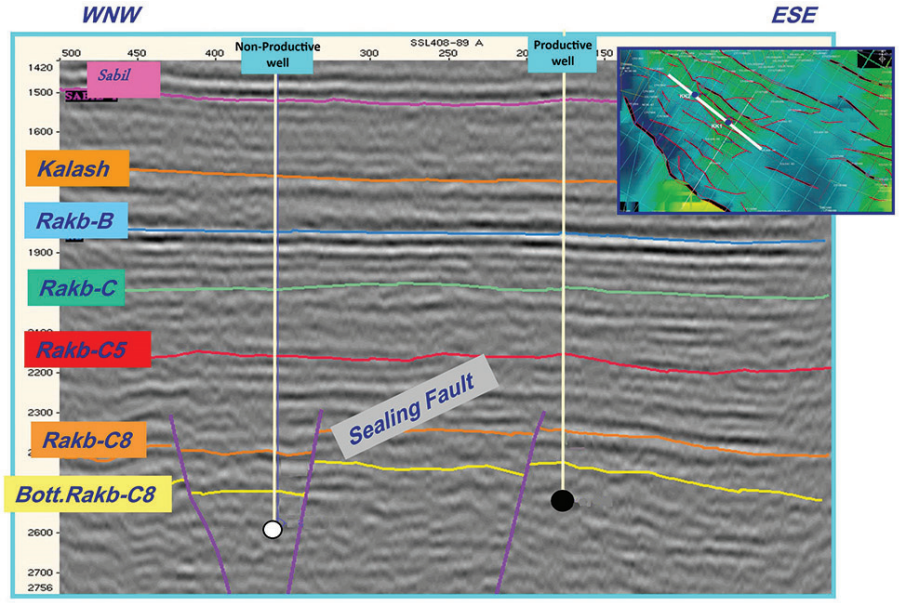

Fig. 5 The NW–SE seismic section illustrates both productive and non-productive wells in the study area, along with fault patterns and domestic reservoirs

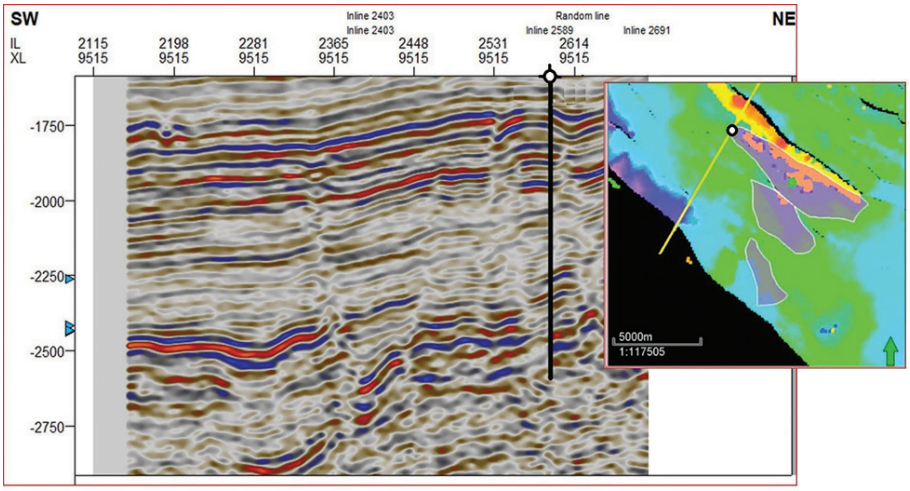

Fig. 6 Seismic cross-line section (SW–NE) intersecting the non-productive well path displays the raw seismic data prior to interpretation

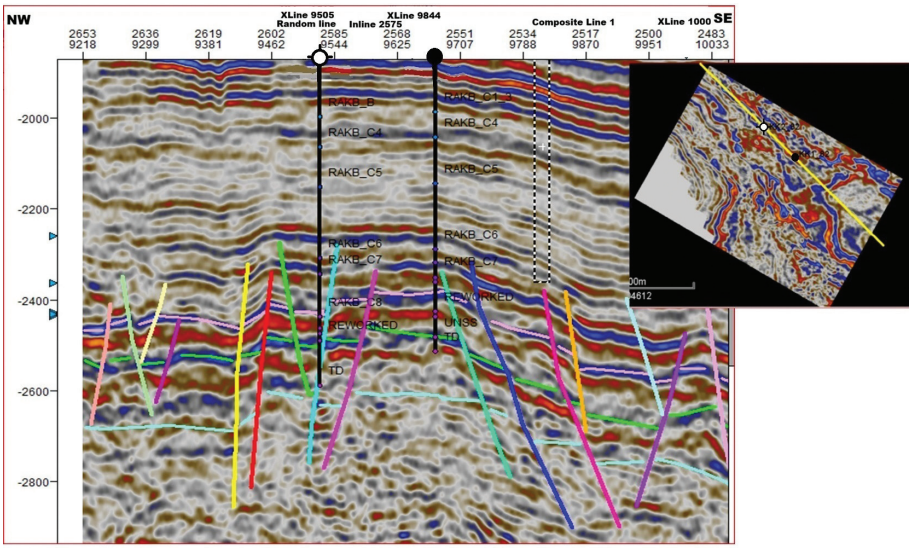

Fig. 7 Seismic line (NW–SE) crossing both productive and non-productive wells; highlights the interpreted faults

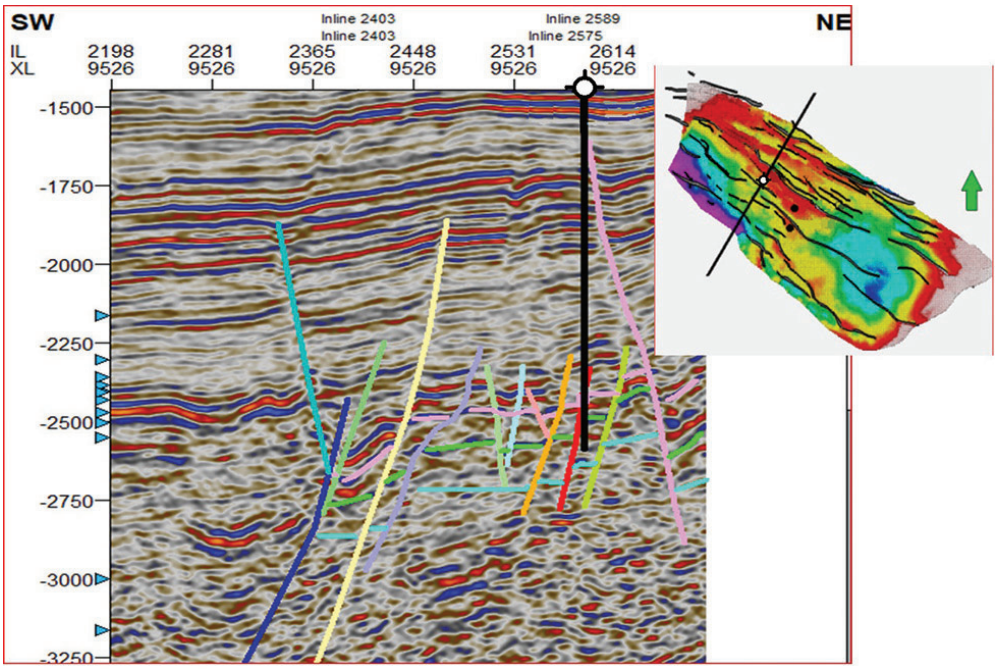

Fig. 8 Seismic line (SW–NE) crossing the non-productive well; highlights the interpreted faults

ful for delineating dominant fault trends and identifying anomalous discontinuities, especially around non-productive wells.

In this study, the variance attribute parameters were tailored based on the observed fault trends. An increase in the inline parameter enhances the detection of faults aligned with the seismic inline direction, and vice versa (Fig. 9). Figure 10 presents a 2D view of the variance attribute slice at the depth of the top reservoir (RC–8), which reveals fracture-related discontinuities near both productive and non-productive wells.

The 3D view (Fig. 11) illustrates a classic seismic crossline intersecting with the fault trends identified in the variance attribute slice at the top reservoir. The 3-D seismic volume covers approximately 441 km², with an inline spacing of 30 m, crossline spacing of 30 m, and a bin size of 30 × 30 m. The dominant frequency ranges from 10–40 Hz, with a peak frequency of approximately 15 Hz. The consistency between the variance attribute results and the original seismic data further validates the interpretation. Additionally, Fig. 12 shows that both the seismic intersection and the variance attribute slice confirm the presence of a fault near the non-productive well at the top reservoir level.

Ant Tracking attributes

Ant Tracking is an advanced technique used in seismic interpretation to detect and trace subsurface geological structures that are often difficult to identify using conventional methods (Silva *et al*. 2005; Zhang *et al*. 2017). Seismic attributes – quantitative representations of seismic data – provide valuable information about subsurface geology, including reflectivity, amplitude, and frequency. Ant Tracking algorithms analyze these attributes to delineate features such as faults, channels, and fractures.

The Ant Tracking algorithm is inspired by the behaviour of real ants and their use of pheromone trails. In the algorithm, virtual ants are deployed across the seismic attribute grid and are allowed to traverse it while depositing virtual pheromones. Areas where pheromone trails accumulate in higher densities are interpreted as indicative of potential subsurface features. These features can then be examined further using additional seismic attributes or geological data.

This technique can be implemented using various software platforms, such as the Ant Tracking Attribute tool in Schlumberger's Petrel software. When integrated with other seismic attributes and geological models, Ant Tracking can enhance subsurface interpretation and support hydrocarbon exploration and production by providing a more comprehensive understanding of structural geology.

Ant Tracking parameters can be configured according to different detection strategies, typically classified as aggressive or passive. For this analysis, an aggressive setting was selected to enhance the detection of subtle and minor faults or fractures. In addition, the parameter configuration was informed by azimuthal inclination to better align with the predominant orientation of geological features. Ant Tracking

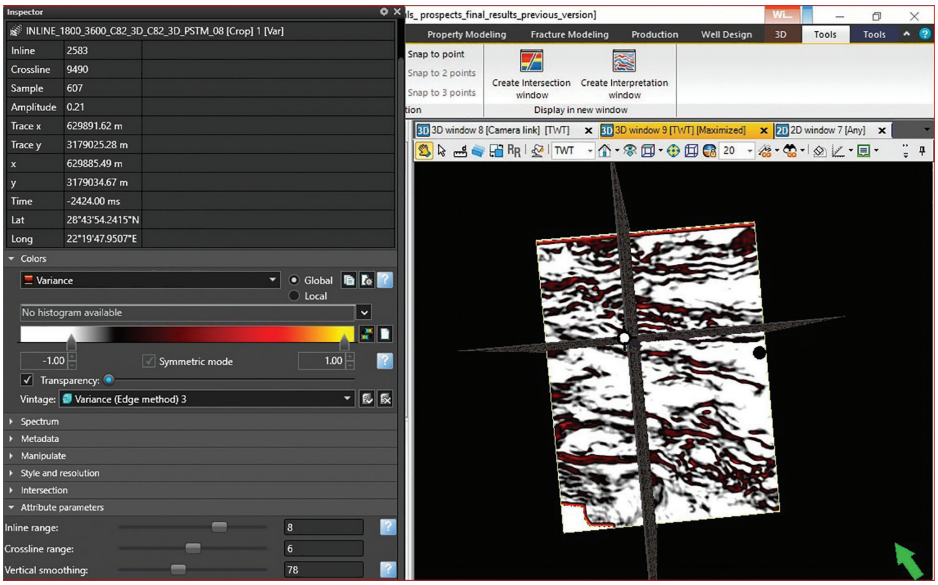

Fig. 9 Applying the variance attribute to the seismic cube enhanced by a median filter

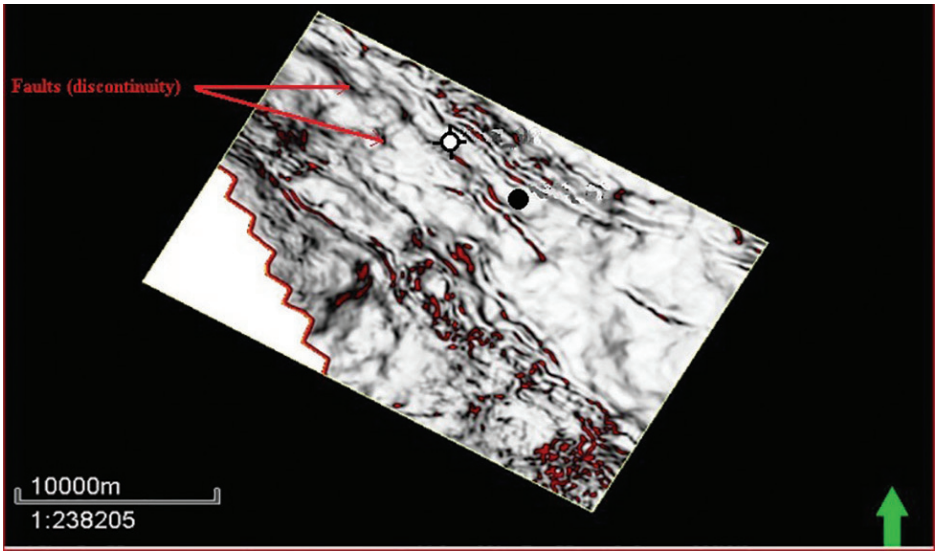

Fig. 10 The 2D view of the variance attribute slice at the depth of the top reservoir (RC_8)

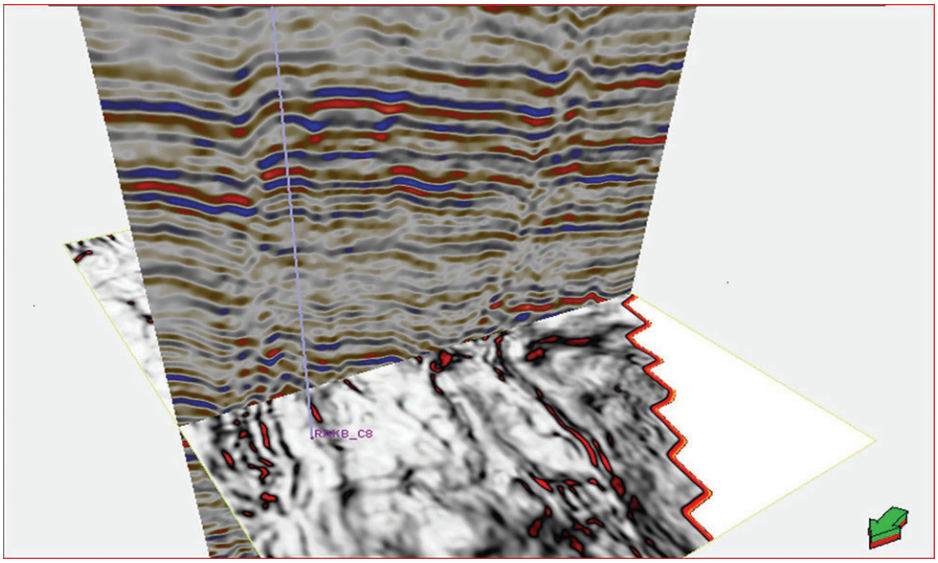

Fig. 11 The 3D view of the original seismic crossline intersecting the fault trends on the variance attribute slice (top RC_8)

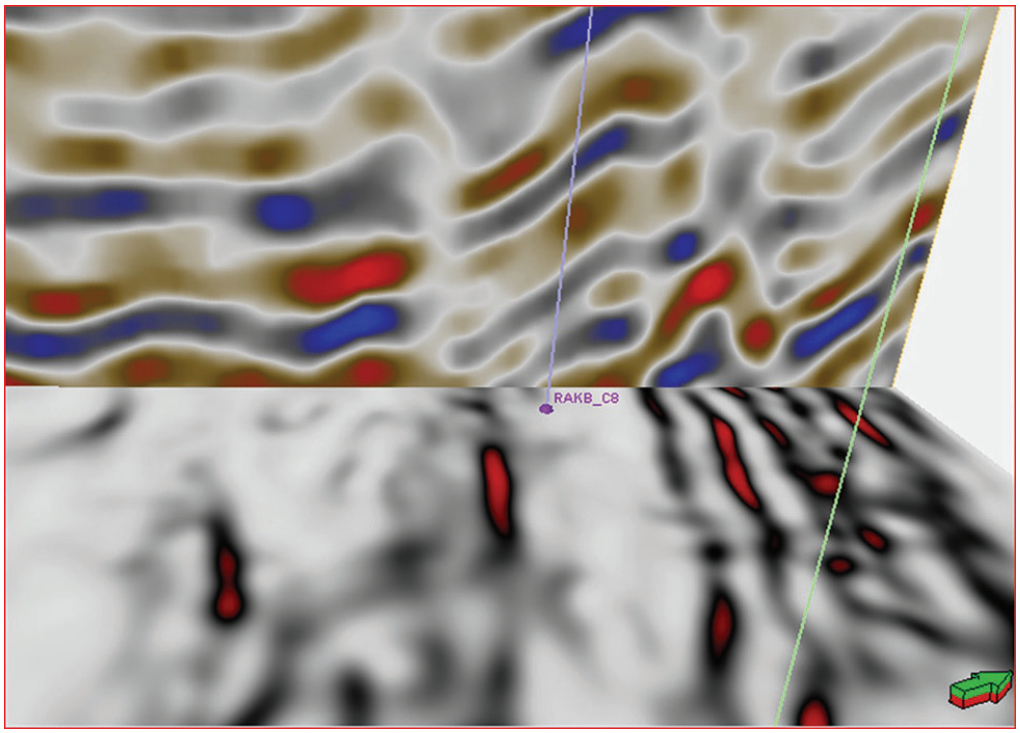

Fig. 12 The 3D view shows that the seismic intersection and variance attribute slice indicate the presence of a fault near the non-productive wellbore at the top of the RC_8 reservoir

enhances the visualization of subtle discontinuities and allows quantitative assessment of fracture intensity, density, and orientation.

To validate the identified faults, interpretations derived from Ant Tracking were compared qualitatively with those from the original seismic data. Particular attention was paid to fault continuity and density. Every identifiable fault was interpreted individually due to its potential impact on drilling and production operations, specifically in mitigating risks such as mud loss during drilling and early water breakthrough during production.

The interpretation process was designed to assess faults across different scales and to evaluate their implications on both static and dynamic reservoir models (Cunha 2003). A qualitative comparison was made between fault interpretations derived from original seismic data and those enhanced through Ant Tracking to assess their relative effectiveness in identifying critical structural features.

Ethical and operational considerations were central to the fault interpretation process, especially concerning the safety and efficiency of drilling and production activities. A well-by-well interpretation approach was employed to ensure no significant faults were overlooked – faults that could pose a risk to operations. Notably, the dominant fault trends identified in the original seismic data were used as a reference framework to verify the existence of less obvious or ambiguous faults highlighted by the Ant Tracking attribute (Fig. 13).

GIS techniques for the analysis of faults

All faults interpreted from the seismic data (Fig. 14) were subjected to statistical analysis using GIS techniques to construct rose diagrams and assess variations in fault orientation, frequency, density, and length. Figure 14 (a) and (b) present rose diagrams illustrating the fault trends extracted from the original seismic data and the Ant Tracking attribute, respectively. Both diagrams highlight the dominant fault trends within the study area.

To generate a fault density map, the Line Density tool was employed (Esri, n.d.). Figures 15 and 16 display the fault density distributions derived from the original seismic data and the Ant Tracking attribute, respectively. The density levels are categorized into three classes: high (red), medium (yellow), and low (green).

RESULTS AND DISCUSSION

By incorporating the Ant Tracking Attribute derived from variance analysis, a total of 373 faults and associated brittle fractures were successfully identified within the study area at the top reservoir level (RC_8). Fault lengths in the study area range from approximately 100 to 400 meters for minor faults and extend up to 800 to 1,200 meters for the major WNW–ESE trending faults. The interpreted faults predominantly exhibited WNW–ESE and NNW–SSE trends, with a secondary trend in the N–S trend interpreted as a frac-

ture population rather than major faulting. These results are consistent with those obtained from the original seismic data, both indicating similar dominant fault orientations within the study area.

The fault density map reveals two distinct distribution patterns. According to the line density map derived from the faults interpreted using the original seismic data, a high-density zone is primarily concentrated in the northern part of the study area (Fig. 15), while the remaining zones exhibit relatively low fault density. In contrast, the line density map generated from the faults extracted using the Ant Tracking Attribute indicates two prominent high-density zones distributed across the study area, predominantly in the northern and southern regions (Fig. 16). The longitudinal blocks of parallel faults observed in the line density maps may suggest the presence of horst and graben structures within the study area.

The rose diagrams (Fig. 14(a) and (b)) indicate that three major fault orientations – WNW–ESE, NNW–

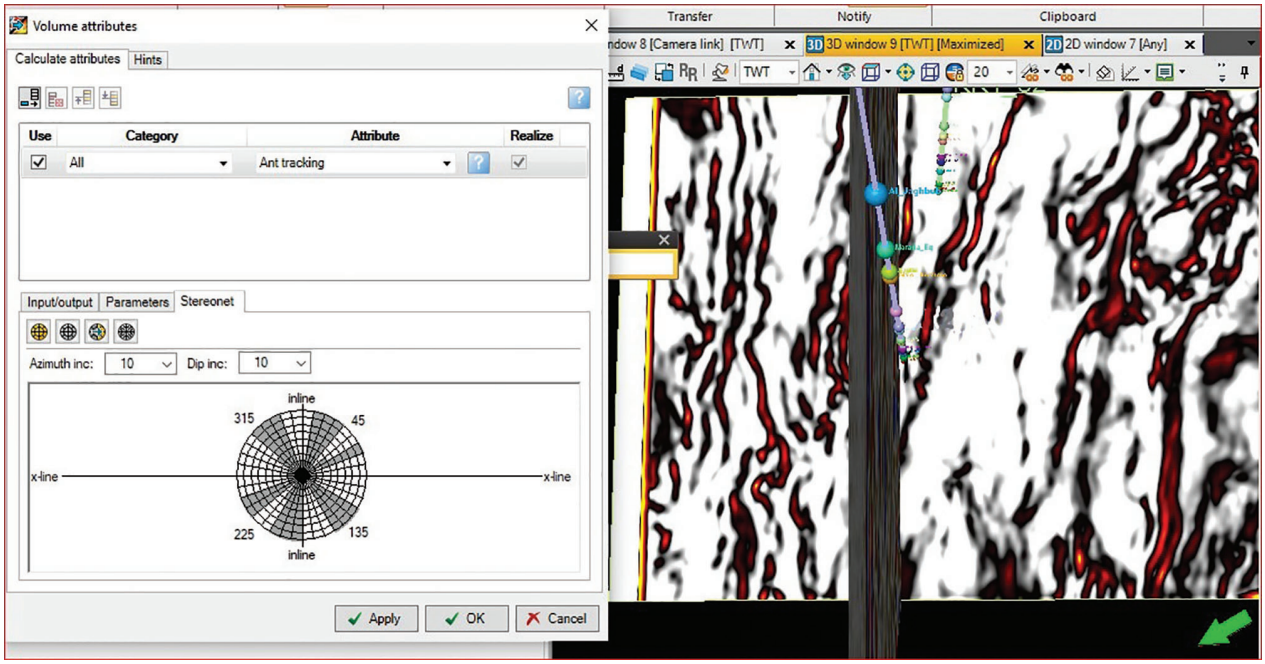

Fig. 13 Selection of Ant Tracking attribute parameters based on the azimuth and inclination angles of dominant fault trends

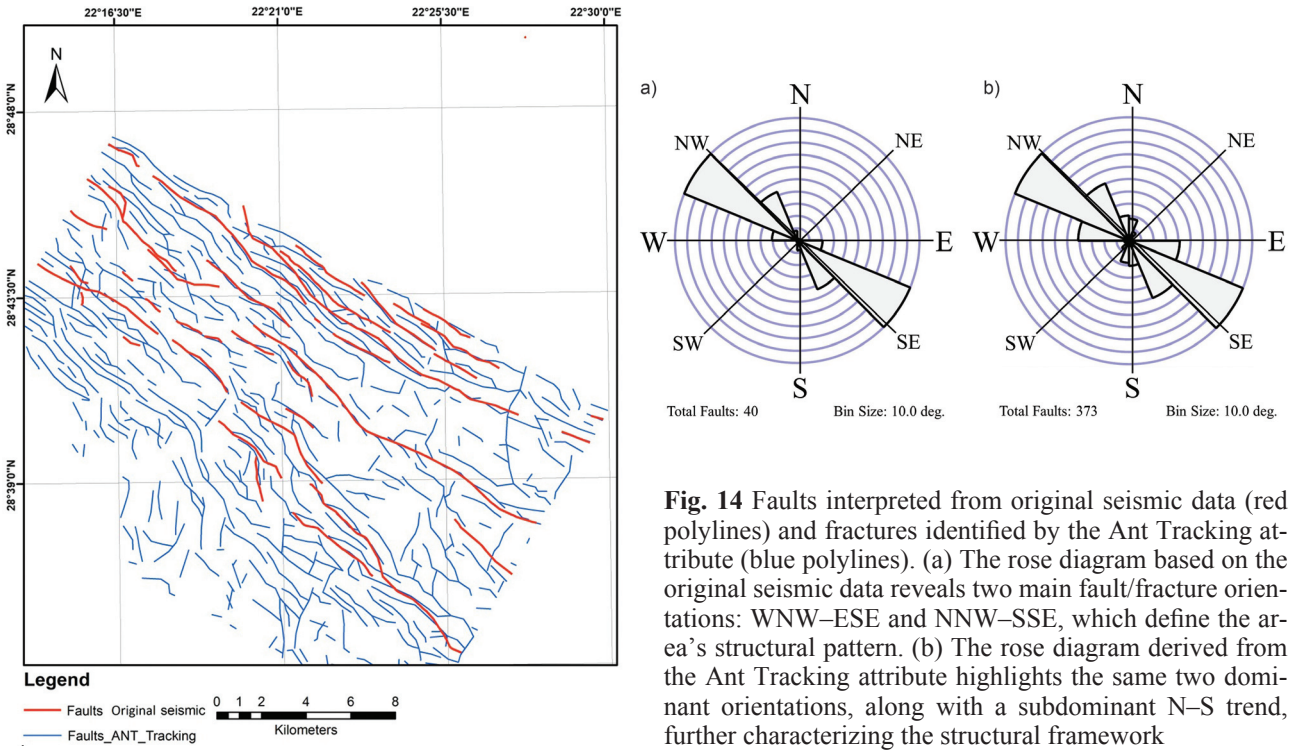

Fig. 14 Faults interpreted from original seismic data (red polylines) and fractures identified by the Ant Tracking attribute (blue polylines). (a) The rose diagram based on the original seismic data reveals two main fault/fracture orientations: WNW–ESE and NNW–SSE, which define the area's structural pattern. (b) The rose diagram derived from the Ant Tracking attribute highlights the same two dominant orientations, along with a subdominant N–S trend, further characterizing the structural framework

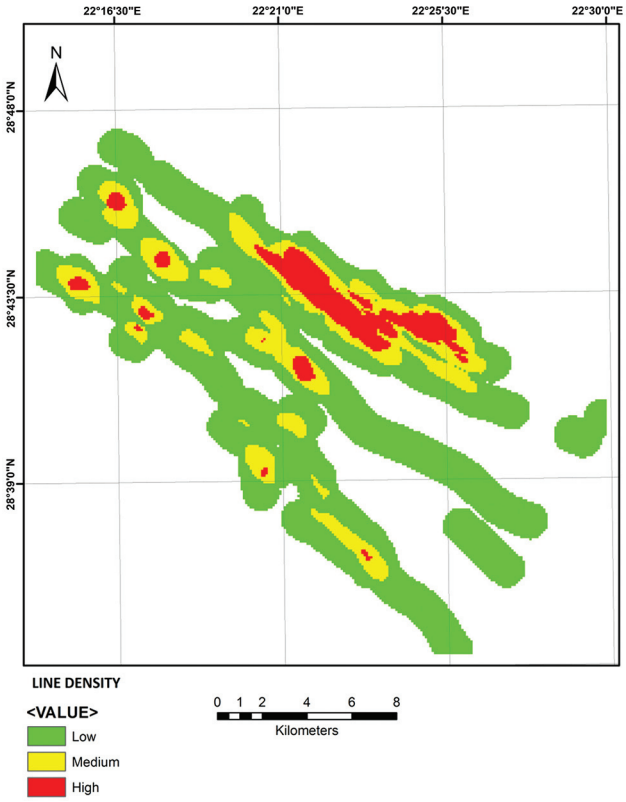

Fig. 15 Lineament density map of RC-8 reservoir faults and fractures extracted from the original seismic data, categorized into three density levels: high (red), medium (yellow), and low (green). The map was generated using a grid of 0.5 × 0.5 km cells with a density radius of 1 km

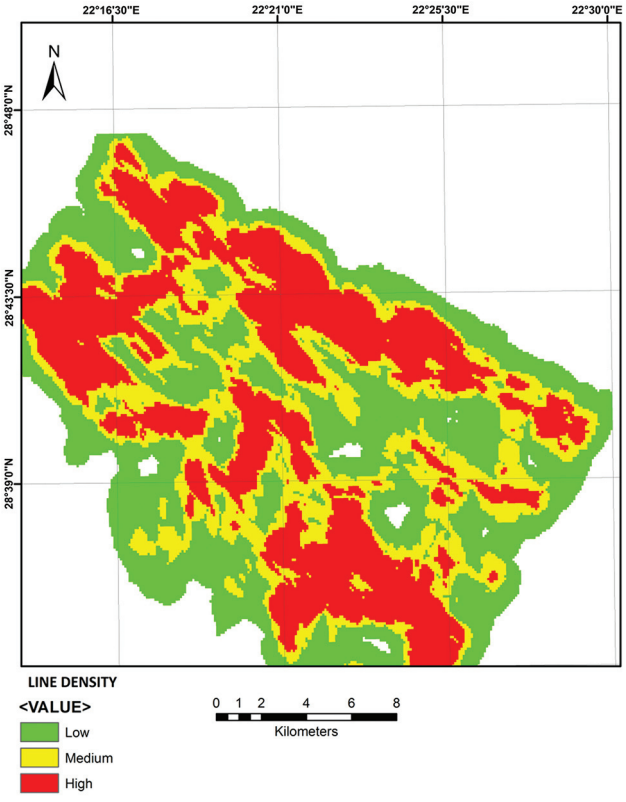

Fig. 16 Lineament density map of RC-8 reservoir faults/fractures extracted from the Ant Tracking attribute, classified into three density levels: high (red), medium (yellow), and low (green). It is computed using a 1 km kernel within the ArcGIS Line Density tool

SSE, and N–S – characterize the study area. The analysis reveals that the dominant subsurface faults trend predominantly in the WNW–ESE to NNW–SSE directions, while the N–S orientation is subordinate. Other orientations are statistically insignificant. The predominance of WNW–ESE trending structures is consistent with an extensional tectonic setting characteristic of the Sirte Basin during Late Cretaceous rifting. These varying fault directions suggest that the Sirte Basin experienced multiple tectonic phases, likely resulting in repeated reactivation of the study area and the generation of distinct fault sets. These findings are consistent with and corroborate numerous previous studies on the Sirte Basin.

To further emphasize and investigate faults near the non-productive wellbore, an efficient zooming method was employed (Fig. 17). This fault is likely a contributing factor to the severe water invasion observed in the non-productive well.

Minor lateral facies variations occur within the Rakb carbonate platform; however, these are less pronounced than the structural discontinuities and do not significantly affect attribute interpretation within the limited study area. Although the Rakb Group comprises multiple subunits, this study focuses exclusively on the RC-8 reservoir, the only interval intersected by both productive and non-productive wells.

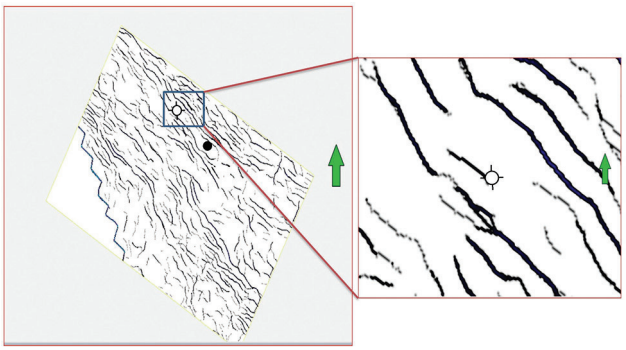

Fig. 17 A zoomed-in image of the non-productive well (indicated by the black circle) reveals the presence of adjacent faults. The green circle denotes the location of the productive well

Notably, the results from the Ant Tracking Attribute align closely with those from the original seismic interpretation, confirming the same fault trends across the area. However, the Ant Tracking Attribute provided a more detailed visualization. A subtle fault near the non-productive wellbore, which was not clear in the original seismic data, was distinctly visualized in the Ant Tracking Attribute slice (Fig. 18). A 3D visualization further illustrates this fault intersecting the non-productive wellbore at the top of the reservoir (Fig. 19).

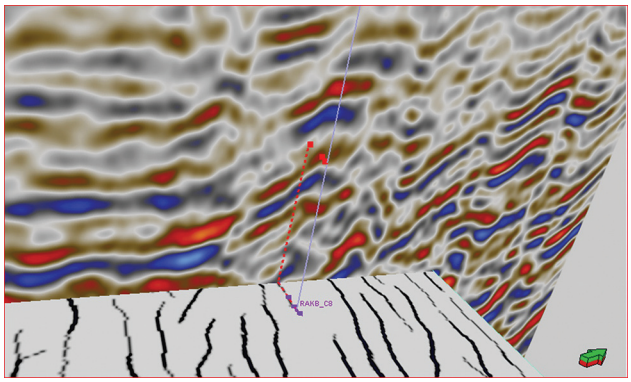

Fig. 18 The 3D view illustrates the original seismic crossline intersecting with the fault trends identified in the Ant Tracking Attribute slice at the top reservoir level. The results show a high degree of consistency

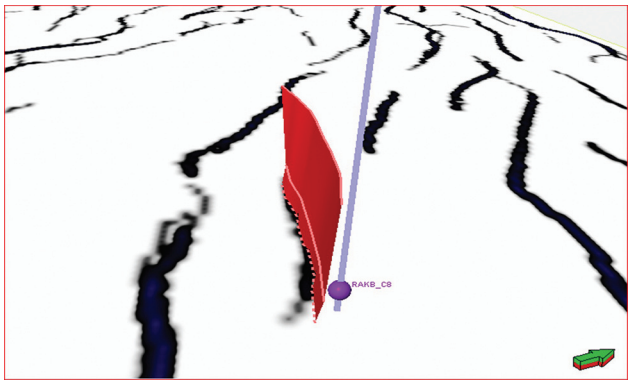

Fig. 19 The 3D view illustrates the fault intersecting the non-productive wellbore at the top of the reservoir

According to Zhao *et al*. (2024), the tectonic evolution of the Sirte Basin can be divided into four main stages:

1. Early Rifting Stage: The basement rocks of the Sirte region belong to the Precambrian Pan-African orogenic belt and exhibit evidence of compressional tectonics. Overlying Paleozoic strata represent a relatively stable cratonic succession with minimal tectonic disturbance (Anketell 1996). During the Triassic to Early Jurassic, the area functioned as a passive margin experiencing thermal subsidence. Rifting commenced in the Middle to Late Jurassic and intensified during the Early Cretaceous (Ahlbrandt 2001), marking the Early Rifting Stage that initiated the development of the proto-Sirt Basin.
2. Early Rifting Stage (Middle-Lower Jurassic): The opening of the Neo-Tethys Ocean led to basin uplift accompanied by large-scale regression. The Sirte Basin subsided during the Late Cretaceous, with rapid marine transgression by the Neo-Tethys Sea. This transgression continued until the Toulon age, followed by further ocean transgression. By the end of the Eocene, the basin experienced complete subsidence with large-scale regression.
3. Late Rifting Stage: During the Late Rifting Stage (Late Cretaceous), extensional deformation intensified mainly in the north-eastern Sirte Basin, while Early Jurassic rifting continued to influence the central and western parts of the basin (Anketell 1996; Ahlbrandt 2001).
4. Post-Rift Stage (Paleogene–Recent): Following the cessation of major extensional tectonics in the Late Cretaceous, the Sirte Basin experienced a prolonged period of thermal subsidence and sedimentary infill from the Paleogene to the present. This Post-Rift Stage is characterized by regionally continuous, relatively undeformed sedimentary packages with minimal fault activity. Normal faults formed during the Jurassic to Early Cretaceous syn-rift phase gradually became inactive, and no significant structural deformation is observed above the Rakb-C5 horizon. During this stage, the deposition was dominated by marine shales, carbonates, and later clastic systems that onlap and drape the older rift architecture. The Post-Rift Stage established the necessary burial, maturation, and sealing conditions for the development of the petroleum system in Concession 82.

Petroleum System Development: In the Sirte Basin, Lower Cretaceous and Paleogene sandstones locally form secondary hydrocarbon reservoirs, whereas the Rakb carbonates represent the primary reservoir interval in the study area. The main source rock is the Upper Cretaceous Sirte Shale, which contains moderate to high TOC values (typically 2–6%). Regional sealing units are composed of thick Upper Cretaceous and Paleogene shales that provide an effective cap rock.

In the same context, Gumati and Nairn (2007) report that the Sirte Basin has experienced faulting and differential subsidence resulting from lithospheric extension over a 25-million-year period beginning in the Late Cretaceous. The initial phase of extension and subsidence, characterized by faulting and graben formation, occurred between the Cenomanian and Campanian stages. This was followed by widespread thermally driven subsidence from the Maastrichtian through the Eocene and Oligocene, accounting for approximately half of the total subsidence.

Detailed reconstructions of basin subsidence, sediment accumulation rates, and facies variations for the northern Sirte Basin have been developed using data from approximately 100 completion well logs and numerous seismic lines. This vertical variation in fracturing indicates that the main phase of faulting occurred during the syn-rift deposition of the Rakb-

C6 and older units, with only limited upward propagation into the younger, post-rift layers (Rakb-C5 and above). These studies reveal that renewed differential subsidence, following fault reactivation, occurred intermittently during the Late Cretaceous and Paleocene–Eocene epochs. Tectonic subsidence maps indicate a systematic southeast-to-northwest migration of the loci of maximum subsidence, paralleling the structural trend of the basin. The greatest subsidence within the Sirte Trough reaches 2,085 meters, while subsidence over the horst blocks generally measures less than 1,000 meters, corresponding to an extension range of 10–75%, with an average extension below 50%. The central graben exhibits the highest degree of stretching.

Lithospheric necking refers to the localized, focused thinning of the continental lithosphere within the central axis of a rift system, producing a narrow zone of strong extension. This differs from regional lithospheric stretching, which involves more distributed and uniform deformation across a broader area. In the Sirte Basin, localized lithospheric necking during the Early–Middle Jurassic produced the deep axial depocenters, while broader regional stretching controlled the later Cretaceous rift development.

Based on these findings, it can be concluded that the non-productive well was drilled at a suboptimal location, likely due to the poor quality of the original seismic data and insufficient site characterization. Furthermore, there is a strong likelihood of hydrocarbon presence in the study area if a well is drilled away from fault plane. The fault density maps derived from the Ant Tracking Attribute provide valuable guidance for selecting an optimal drilling location to improve the chances of discovering a productive well within the study area.

CONCLUSIONS

A fault caused water invasion during previous drilling operations at a well in the study area. Moreover, this fault likely served as a pathway for hydrocarbon migration. Faults with larger throw, greater continuity, and reservoir-on-reservoir contacts are more likely to serve as vertical hydrocarbon migration pathways, while small-throw faults ending within aquifer-bearing intervals may act as preferential conduits for water.

This study aimed to extract, interpret, and evaluate faults adjacent to both productive and non-productive wells by using seismic data and GIS techniques. The primary objective was to identify faults and fractures within the study area to optimize well placement and minimize the risk of water invasion during future drilling operations.

Seismic data analysis indicates that the non-productive well was drilled directly on a fault plane, which is the primary cause of water invasion. The poor quality of the original seismic data hindered the detection of such faults prior to drilling.

Fault analysis reveals two dominant fault orientations in the study area: WNW–ESE and NNW–SSE. The WNW–ESE trending fault-fracture system clearly dominates the structural fabric of the study area, consistent with Late Cretaceous extensional tectonics. These varying fault trends suggest that the Sirte Basin has undergone multiple tectonic phases, likely resulting in repeated reactivation of faults and the development of distinct fault sets. These observations are consistent with findings from previous studies on the Sirte Basin (Abdunaser, McCaffrey 2015).

Fault density maps highlight two high-density zones located in the northern and southern parts of the study area. The presence of WNW–ESE fault blocks arranged in parallel, as revealed by the line density maps, suggests the potential occurrence of horst and graben structures within the study area.

The results demonstrate the feasibility of drilling a pilot well in the study area, provided that the faults in the region are adequately and accurately studied to avoid operational complications. Techniques such as the Ant Tracking Attribute can effectively minimize the adverse impact of faults and fractures on drilling operations and production efficiency. Additionally, it is highly recommended to integrate data by using rose diagrams and fault density maps at both the field and basin scales to reduce geological uncertainties and prevent drilling challenges.

ACKNOWLEDGMENTS

The authors gratefully acknowledge the anonymous reviewers and the editor for their valuable comments and feedback, which significantly enhanced the quality of the manuscript.

Conflict of interests

The authors declare that they have no conflicts of interest.

Author contributions

The authors contributed equally to the study's conception, design, data analysis, and manuscript preparation.

REFERENCES

Abdalla, M. 2021. Seismic attributes aided detection of NW–SE trending faults developed on an isolated carbonate platform in the NW Sirte Basin, North Central Libya. *International Journal of Engineering Applied Sciences and Technology 5(11), 31–43*. https://doi.org/10.1190/SEGAM2017-17431339.1

Abdullah, N., Hasan, N., Saeid, N., Mohyaldinn, M.E., Zahran, E.S.M.M. 2020. The study of the effect of fault transmissibility on the reservoir production using reservoir simulation – Cornea Field, Western Australia. *Journal of Petroleum Exploration and Production Technology 10,* 739–753. https://doi.org/10.1007/s13202-019-00791-6

Abdunaser, A.E., McCaffrey, K.J.W. 2015. Tectonic history and structural development of the Zallah-Dur al Abd Sub-basin, western Sirt Basin, Libya. *Journal of Structural Geology 73*, 46–65. https://doi.org/10.1016/j.jsg.2015.02.006

Ahlbrandt, T.S. 2001. The Sirte Basin Province of Libya – Sirte-Zelten Total Petroleum System. *U.S. Geological Survey Bulletin 2202–F,* 29. https://doi.org/10.3133/b2202F

Ambrose, G. 2000. The geology and hydrocarbon habitat of the Sarir Sandstone, SE Sirt Basin, Libya. *Journal of Petroleum Geology 23,* 165–192. https://doi.org/10.1111/j.1747-5457.2000.tb00489.x

Anketell, J.M. 1996. Structural history of the Sirt Basin and its relationships to the Sabratah Basin and Cyrenaican Platform, Northern Libya. In: Salem, M.J., El-Hawat, A.S., Sbeta, A.M. (Eds), *The geology of Sirt Basin*. Amsterdam, Elsevier, *III*, 57–88.

Azzam, S.S., Elkady, H.H, Rabea, T.M. 2018. The impact of seismic interpretation on the hydrocarbon trapping at Falak field, Meleiha, Western Desert, Egypt. *Egyptian Journal of Petroleum 27(4)*, 785–793. https://doi.org/10.1016/j.ejpe.2017.11.006

Cunha, L.B. 2003. Integrating Static and Dynamic Data for Oil and Gas Reservoir Modelling. *Journal of Canadian Petroleum Technology 43,* 8–11. https://doi.org/10.2118/2003-219

Esri. (n.d.). Line Density (Spatial Analyst). ArcGIS Pro Documentation. Retrieved June 7, 2025. https://pro.arcgis.com/en/pro-app/latest/tool-reference/spatial-analyst/line-density.htm

Fernandez-Ibanez, F., Nolting, A., Breithaupt, C.I., Darby, B., Mimoun, J., Henares, S. 2022. The properties of faults in the Brazil pre-salt: A reservoir characterization perspective. *Marine and Petroleum Geology 146, 105955*. https://doi.org/10.1016/j.marpetgeo.2022.105955

Futyan, A., Jawzi, A.H. 1996. The hydrocarbon habitat of the oil and gas fields of North Africa with emphasis on the Sirt Basin. In: Salem, M.J., El-Hawat, A.S., Sbeta, A.M. (Eds), *The geology of Sirt Basin*. Amsterdam, Elsevier *II*, 287–308.

Gras, R. 1996. Structural style of the southern margin of the Messlah High. In: Salem, M.J., El-Hawat, A.S., Sbeta, A.M. (Eds), *The geology of Sirt Basin*. Amsterdam, Elsevier *III*, 201–210.

Gras, R., Thusu, B. 1998. Trap architecture of the Early Cretaceous Sarir Sandstone in the eastern Sirt Basin, Libya. *Geological Society, London, Special Publications 132*, 317–334. https://doi.org/10.1144/GSL.SP.1998.132.01.18

Guiraud, R., Bosworth, W. 1997. Senonian basin inversion and rejuvenation of rifting in Africa and Arabia – Synthesis and implication to plate-scale tectonics. *Tectonophysics 282,* 39–82. https://doi.org/10.1016/S0040-1951(97)00212-6

Gumati, Y.D., Nairn A.E.M. 2007. Tectonic subsidence of the Sirte Basin, Libya. *Journal of Petroleum Geology 14(1),* 93–102. https://doi.org/10.1111/j.1747-5457.1991.tb00301.x

Harding, T.P. 1984. Graben hydrocarbon occurrences and structural styles. *American Association of Petroleum Geologists 68(3),* 333–362. https://doi.org/10.1306/AD460A21-16F7-11D7-8645000102C1865D

Jaglan, H., Qayyum, F., Hélène, H. 2015. Unconventional seismic attributes for fracture characterization. *First Break 33(3),* 20–25. https://doi.org/10.3997/1365-2397.33.3.79520

Kim, M., Yu, J., Kang, N.-K., Kim, B.-Y. 2021. Improved Workflow for Fault Detection and Extraction Using Seismic Attributes and Orientation Clustering. *Applied Sciences 11(18),* 8734. https://doi.org/10.3390/app11188734

Kroner, A. 1993. The Pan-African belt of northeastern and eastern Africa, Madagascar, southern India, Sri Lanka and east Antarctica; Terrane amalgamation during formation of the Gondwana Supercontinent. In: Thorwiehe, U., Schandelmeier, H. (Eds), *Geoscientific research in Northeast Africa*. Rotterdam, Netherlands, A.A. Balkema, 3–9. https://doi.org/10.1201/9780203753392

Liu, Y.K. 2013. Noise reduction by vector median filtering. *Geophysics 78,* 79–86. https://doi.org/10.1190/geo2012-0232.1

Magoon, L.B., Dow, W.G. 1994. The petroleum system – From source to trap. *American Association of Petroleum Geologists 60,* 3–23. https://doi.org/10.1306/M60585

Mansour, A.T., Magairhy, I.A. 1996. Petroleum geology and stratigraphy of the southeastern part of the Sirt Basin, Libya. In: Salem, M.J., El-Hawat, A.S., Sbeta, A.M. (Eds), *The geology of Sirt Basin*. Amsterdam, Elsevier *II*, 485–528.

MOGCO. 2019. Reservoir Description. *Internal Report*, Mellitah Oil & Gas B.V., Libyan Branch, Tripoli, Libya, 2019.

Onajite, E. 2014. *Seismic Data Analysis Techniques in Hydrocarbon Exploration*. Amsterdam, Netherlands: Elsevier. https://doi.org/10.1016/B978-0-12-420023-4.00001-0

Popovici, A.M., Fomel, S., Abdelnabi, A., Liu, K., Gao, S., Abushalah, Y. 2017. Seismic attributes aided fault detection and enhancement in the Sirte Basin, Libya. *SEG Technical Program Expanded Abstracts 2017,* 2340–2344. https://doi.org/10.1190/segam2017-17431339.1

Shaltami, O., Alghamari, H., Hkoma, M. 2025. Elemental Geochemistry of the Upper Cretaceous Rakb Formation in Well C3-65, Sarir Field, Sirte Basin, NE Libya. *Derna Academy Journal for Applied Sciences 4(4),* 64–84. https://doi.org/10.71147/mmpnge431

Shoup, R. 2019. A Corporate Strategy for Reducing Dry Holes and Improving Resource and Reserve Estimates.

2019 AAPG Annual Convention and Exhibition, San Antonio, Texas. https://www.searchanddiscovery.com/abstracts/html/2019/ace2019/abstracts/168.html

Silva, C.C., Marcolino, C.S., Lima, F.D. 2005. Automatic fault extraction using ant tracking algorithm in the Marlim South Field, Campos Basin. In: *SEG Technical Program Expanded Abstracts 2005,* 219–223. Society of Exploration Geophysicists. https://doi.org/10.1190/1.2148294

Zhang, T., Lin, Y., Liu, K., Alhakeem, A. 2017. Fault visualization enhancement using ant tracking technique and its application in the Taranaki basin, new Zealand. In: *SEG Technical Program Expanded Abstracts 2017,* 2350–2354. Society of Exploration Geophysicists. https://doi.org/10.1190/segam2017-17654531.1

Zhao, N., Xiao, Ky., Chen, Zm., Du, Yb., Zheng, Fy., Li, Zh. 2024. Tectonic Sedimentary Evolution and Hydrocarbon Accumulation in Sirte Basin. In: Lin, J. (Ed.) *Proceedings of the International Field Exploration and Development Conference 2023. IFEDC 2023. Springer Series in Geomechanics and Geoengineering*. Springer, Singapore. https://doi.org/10.1007/978-981-97-0464-4_9

Zou, J., Liu, G., Ma, Q., Yu, F., Meng, L., Tian, B. 2023. Analysis of fault characteristics and oil and gas enrichment differences in the No. 2 structural belt, Nanpu Sag, Bohai Bay Basin, East China. *Frontiers in Earth Science 10,* 1057660. https://doi.org/10.3389/feart.2022.1057660